CHAPTER 4

DESIGN AND SIMULATION INVESTIGATIONS OF S-BAND RBWO WITH SECTIONAL BRAGG REFLECTOR

CONTENTS

CHAPTER 4: DESIGN AND SIMULATION INVESTIGATIONS OF S-BAND RBWO WITH SECTIONAL BRAGG REFLECTOR

4.1 Introduction

The gaussian radiation pattern is obtained by radiating the RF energy in TE mode only. In most of the HPM devices, the RF energy is radiated in TM mode, due to this the modulation RF energy produces null on axis. The null on the axis of the radiation pattern is not suitable for HPM applications. Most of the HPM sources are operated in the lower order azimuthally symmetric modes like TM_{0n} mode that has low risk of RF breakdown, due to the lower electric field with high group velocity. It also useful for the operation of the device with high pulse repetition rate. The operating wave of TM_{01} wave is generated with the wave traveling in the opposite direction of the electron beam with negative group velocity. Therefore, the following techniques are used to extract the electron beam axially (i) the cut-off neck reflector can be used for the radiation of RF energy to extract axially and we get any type of mode from backward propagating TM mode at the output by adjusting radius and length of the reflector. The disadvantage of the cut-off neck reflector is that the electron beam is close to the radius of the reflector, which causes pulse shortening, (ii) a resonant reflector (Rectangular RR and Trapezoidal RR) can be used to extract TM modes axially, but this is required an extra mode converter to convert TM mode into TE mode for getting a Gaussian radiation pattern, and (iii) a Bragg structure can be used to reflect the backward propagating wave: it can radiate TE mode without additional mode converter for a long pulse duration. Therefore, in the present work, an RBWO with Bragg structure as a reflector to generate GW level power up to pulse duration 100 ns is proposed.

Abubakirov *et.al*. [111] have initially developed RBWO with Bragg structure as selective mode converter. It was experimentally investigated with a beam energy of 0.8 MV and a produced beam current of 6 kA. An average RF output power of 700 MW with a conversion efficiency of 15 % was obtained in a TE mode output under the guiding magnetic field of 0.7 T with a pulse duration up to 100 ns. Qiao-Sheng *et.al* [91] have simulated an RBWO using Bragg- reflector with sinusoidal guiding magnetic field of 0.68 T at 9.57 GHz, which predicted an RF microwave output power of 1.33 GW for the DC input of 740 kV, 6.5 kA. The conversion efficiency of 27.65 % was achieved in TM_{01} output mode. Qiao-Sheng *et.al* [91] experimentally developed an RBWO with Bragg reflector under the sinusoidal guiding magnetic field of 0.54 T at 9.1 GHz. An RF output power of 0.95 GW was achieved in TM_{01} mode with a conversion efficiency of ~15 %, for the corresponding beam parameters of 800 kV, 8 kA. Elfrgani *et. al* [97] have designed and studied an RBWO outputting a linearly polarized radiation patten using Bragg reflector with an RF output power of 350 MW and a power conversion efficiency of 16.5 %.

In this chapter, the design and simulation of a single frequency RBWO with a new combinational configuration of sectional Bragg reflector and uniform SWS is proposed. The proposed sectional Bragg reflector consists of a sectional sinusoidally helically corrugated cylindrical waveguide. It decreases the RF field around the surface of SWS and helps in increasing the pulse duration of the generated microwave wave. The fundamental and lowest azimuthal symmetric mode TM_{01} is selected as an operating mode to avoid the mode competition issue within the device. The subassemblies of RBWO consists a sectional Bragg reflector for the direct generation of TE_{11} mode, an explosive emission cathode, drift section, SWS, and a tapered collector, as shown in Figure 4.1.

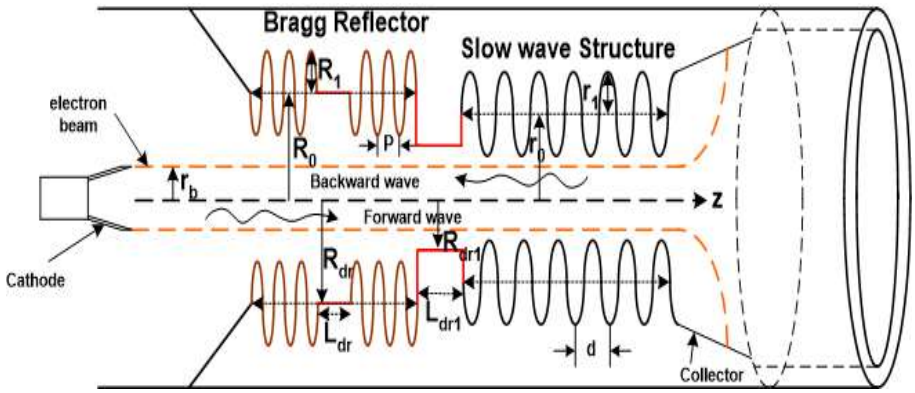

Figure 4.1: 2D Model of Dual-Band RBWO using Bragg Structure.

4.2 Bragg Reflector

The Bragg structure is very effective in millimeter and sub-millimeter wavelength ranges. The effect of mode conversion, and band formation observed in Bragg structures is due to the constructive and destructive interference of wave components caused by periodic disturbances near the Bragg resonance [147]. In the present work, a sectional sinusoidally helically corrugated cylindrical waveguide is designed with zero and non-zero azimuthal index periodic SWS depending upon the desired mode of coupling and conversion. This structure exhibits a stop band which appears at a frequency where the period of Bragg structure is approximately equals to the wavelength.

4.2.1 Design Methodology

In the present design, a sectional Bragg structure is used as reflector cum mode converter. It convert/reflect backward TM_{01} wave to TE_{11} wave in the forward direction, *i.e.*, towards the collector section. The profile of the Bragg structure has been explained in chapter 2.3.2 and sectional Bragg reflector as shown in Figure 4.2. The drift section separates the first and second half section of the of the Bragg structure, whose length is calculated approximately half wavelength of the operating frequency.

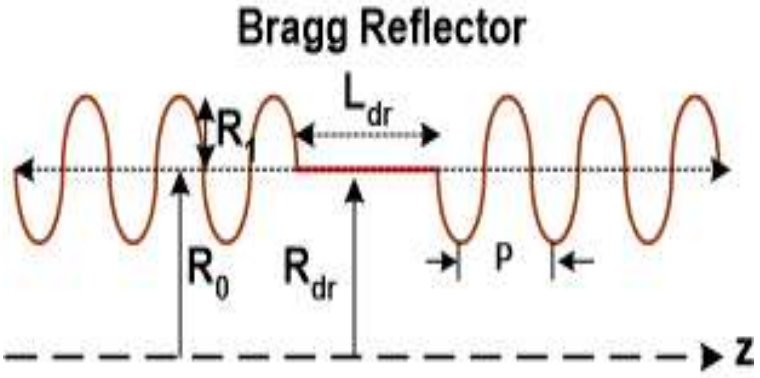

Figure 4.2: (a) 2D longitudinal cut view of Sectional Bragg Structure.

The present work, a single fold Bragg is used to reflect the backward propagating TM_{01} mode and to convert and couple into a forward propagating TE_{11} mode. Based on the coupling, interconversion and reflection for the mode of interest the number of fold for Bragg structure is chosen. The axial period of first and second half section of Bragg structure is calculated as,

$$P = 2\pi / \bar{k}, \tag{4.2}$$

where $\bar{k} = \bar{k}_H + \bar{k}_E$, which can calculate as

$$\bar{k}_H = \sqrt{\left(\frac{\omega}{c}\right)^2 - \left(\frac{\chi_H}{R_0}\right)^2}, \tag{4.3}$$

$$\bar{k}_E = \sqrt{\left(\frac{\omega}{c}\right)^2 - \left(\frac{\chi_E}{R_0}\right)^2} \tag{4.4}$$

where, χ_E and χ_H are the eigen value of TM_{mn} and TE_{mn} modes of consideration, respectively. Finally, the angle of helical corrugation can be calculated as

$$\psi = \tan^{-1}\left(\frac{P}{2\pi R_{\max}}\right) \tag{4.5}$$

4.2.2 Coupling Coefficient and Power Reflection/Conversion Coefficient

The coupling between two modes for the Bragg Structure is decided by the coupling coefficient parameter (δ). The coupling between two modes inside the helical waveguide is given by [148],

for two TE modes,

$$\delta_{E,H} = \frac{R_1}{2R_0^3} \frac{-\chi_E^2 \chi_H^2 + m_E m_H R_0^2 (k^2 + \bar{k}_E \bar{k}_H)}{\sqrt{\bar{k}_E \bar{k}_H} \sqrt{(\chi_E^2 - m_E^2)(\chi_H^2 - m_H^2)}} \tag{4.6}$$

for two TM modes,

$$\delta_{E,H} = \frac{R_1}{2R_0} \frac{(k^2 + \bar{k}_E \bar{k}_H)}{\sqrt{\bar{k}_E \bar{k}_H}} \tag{4.7}$$

and for TM – TE modes

$$\delta_{E,H} = \frac{R_1}{2R_0} \frac{k m_H h}{\sqrt{\bar{k}_E \bar{k}_H (\chi_H^2 - m_H^2)}}, \tag{4.8}$$

where, $k = \omega/c$ is wave number in free space. The dispersion curve will intersect for the resonant coupling of two waves, which occurs between one of the waves and a spatial harmonic of the second wave. Finally, the conversion coefficient or power reflection coefficient is calculated by,

$$K_p = K_{E,H}^2 \tag{4.9}$$

where,

$$K_{E,H} = \tanh(\delta L) \; ; \; L = N \times P \tag{4.10}$$

The present design is dealing with the conversion or coupling of TM_{mn} mode to TE_{mn} mode as RBWO outputted TM_{0n} mode.

Figure 4.3 shows the variation of reflection or conversion coefficient with respect to the number of Bragg axial periods. It is observed that the curve is almost got saturated to one after $N = 6$, hence the number of Bragg axial periods are chosen to be six for minimizing the losses. The design parameters for the sectional Bragg structure are calculated based on above design equations and listed in Table 4.1. The sectional Bragg structure is having a total of six periods (three periods for each section) with separation of drift section.

Table 4.1: Design Parameters of Sectional Bragg Reflector.

Parameters		**Symbol**	**Value**
Bragg Structure (m = ± 1)	Bragg Mean radius	R_0	54.80 mm
	Bragg corrugation amplitude	R_1	06.75 mm
	Bragg Period	P	49.70 mm
	Bragg length	L_{Bragg}	6*P
	Drift Section Length	L_{dr}	47.30 mm

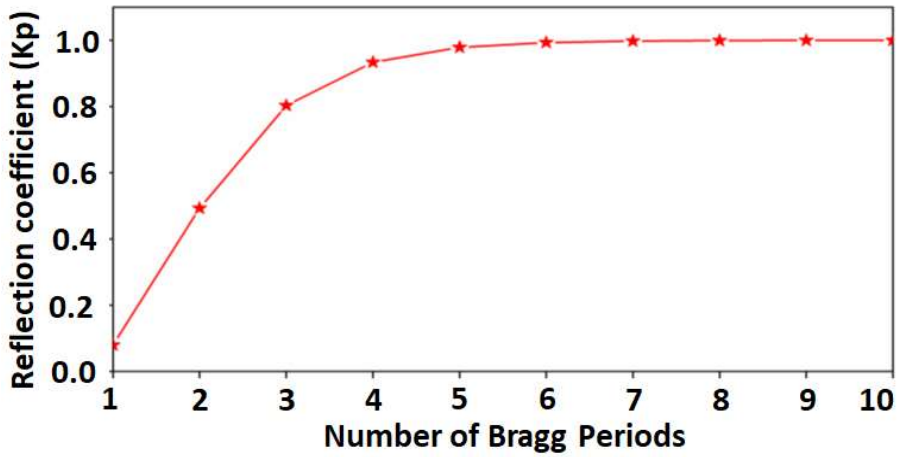

Figure 4.3: Reflection or conversion coefficient vs number of Bragg axial periods.

4.2.3 Cold analysis of Sectional BRAGG Structure

The dispersion relation is one of the important aspects to be obtained for microwave VEDs and HPM sources. The intersection of the beam mode line with the waveguide mode line gives an approximate operating point of the device. The dispersion relation

for two oppositely propagating coupled mode waves within the helically corrugated waveguide is given by [148, 149],

$$(k^2 - k_{\perp E}^2 - \bar{k}_E^2)(k^2 - k_{\perp H}^2 - \bar{k}_H^2) = 4\delta_{E,H}^2 k_0^2, \tag{4.11}$$

where, k_E and k_H are the wavenumbers corresponds to the cut-off frequency of TM_{mn} and TE_{mn} modes, respectively, k_0 is the wavenumber corresponds to an exact Bragg resonance, $k=\omega/c$, and $\delta_{E,H}$ is the coupling coefficient of the TM_{mn} and TE_{mn} waves, respectively. The present case is mainly deal with the conversion and coupling of TM_{01} mode into TE_{11} mode for Gaussian output. The dispersion diagram for sectional Bragg structure is shown in Figure 4.4. The coupling of the desired TE_{11} mode and the -1st space harmonic of the TM_{01} mode is shown to be below the resonant frequency of the SWS [Figure 4.4].

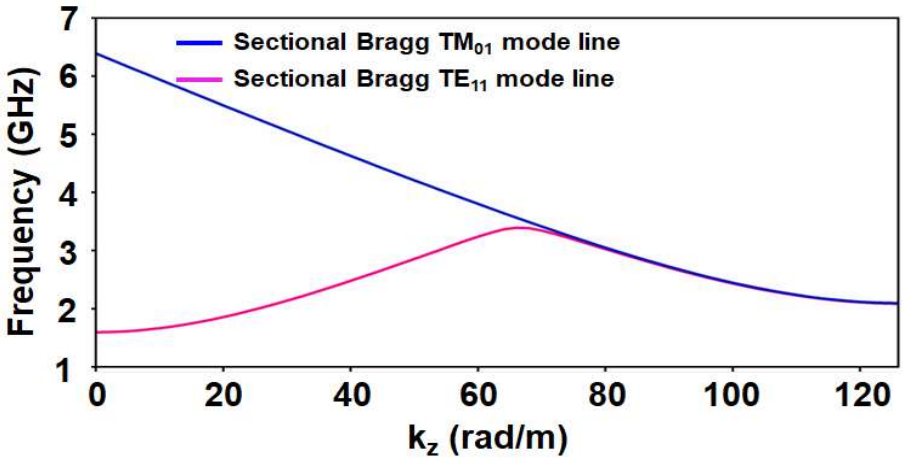

Figure 4.4: Dispersion diagram of Sectional Bragg reflector.

4.3 Slow Wave Structure (SWS)

To generate the S-band microwave with TM_{01}, a cylindrical SWS is chosen with an inner sinusoidal rippled wall having the profile as,

$$r_w = r_0 + r_1 \sin(\bar{k}z + m\phi) \tag{4.12}$$

where, r_0 and r_1 is mean radius and corrugation depth, respectively, m is fold number, and $\bar{k} = 2\pi / d,$ where, d is the period of SWS. The interaction between the -1st spatial harmonic of the backward TM_{01} wave and electron beam in the SWS is observed at ~3.6 GHz, as shown in Figure 4.5. The detailed design of SWS was already explained in Chapter 2. The designed parameters of the SWS are listed in Table 4.2.

Table 4.2: Design Parameters of SWS.

Parameters		**Symbol**	**Value**
Slow Wave Structure (SWS)	SWS Mean radius	r_0	44.80 mm
	SWS Ripple amplitude	r_1	05.10 mm
	SWS Period	d	39.15 mm
	SWS length	L_{sws}	7*d mm
	SWS frequency	f_1	3.6 GHz

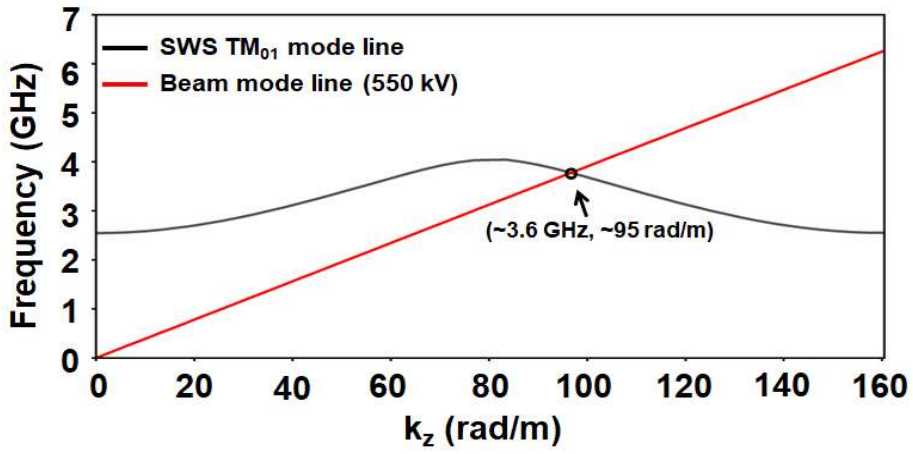

Figure 4.5: Dispersion Diagram of Bragg Structure.

4.4 Modelling of PIC Simulation Results

The RBWO using Bragg Structure is modeled using FDTD based electromagnetics computational software MAGIC-3D, as shown in Figure 4.6. The graphite annular cathode is used for EEE due to its numerous advantages like lower threshold emission field, high melting point and copious emission of electrons. A sectional Bragg reflector section having a cut-off frequency less than the operating frequency of SWS, which is

added nearer to the cathode to enhance the overall efficiency and reduce the wave propagation towards the cathode. Two drift sections are included; drift section-1 is at the middle of Bragg periods and drift section-2 is between the SWS-1 and Bragg reflector, to improve the synchronism condition between the slow space charge wave associated with the beam and RF wave. FUNCTIONAL VOLUME command is used to make the SWS inside the outer CONDUCTOR. The PRESET command is used to set the constant external guiding magnetic field of 1.3 T and AREA along with PORT command is used to set the input-output ports. AREAs and LINEs are made to measure the field voltages and current at the required place. The DC input of 550 kV [Figure 4.7 (a)] is incident on the annular cathode using EXPLOSIVE EMISSION command to emit the hollow electron beam. The developed electron beam current is measured by the command OBSERVE EMITTED ELECTRON CURRENT and is about ~4.66 kA [Figure 4.7 (b)]. The electron beam traverses through the SWS, where the beam- wave interaction takes place, and RF power generated. The generated microwave power is measured by OBSERVE FIELD POWER S. DA STEP FILTER TAVG command at the output port, and it is about ~1.0 GW with a power conversion efficiency of ~39.5 %, as shown in Figure 4.8. The FFT of generated microwave is calculated by using

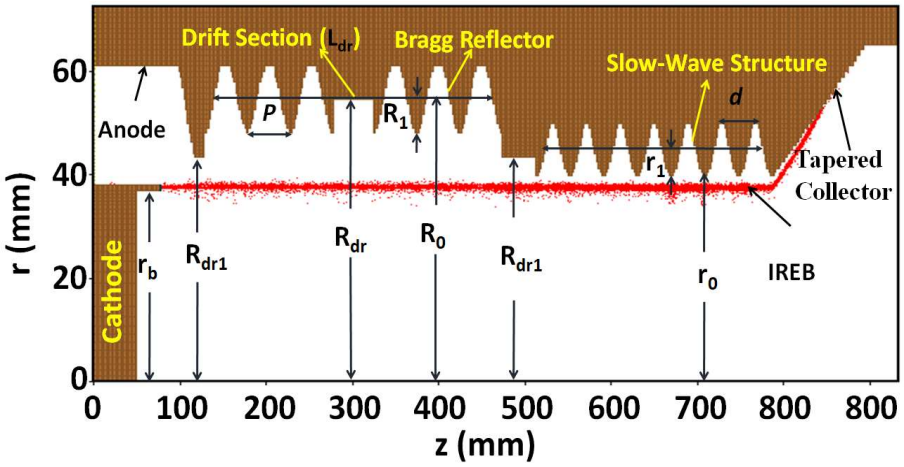

Figure 4.6: 2D simulation configuration of the RBWO with sectional Bragg reflector and IREB particles.

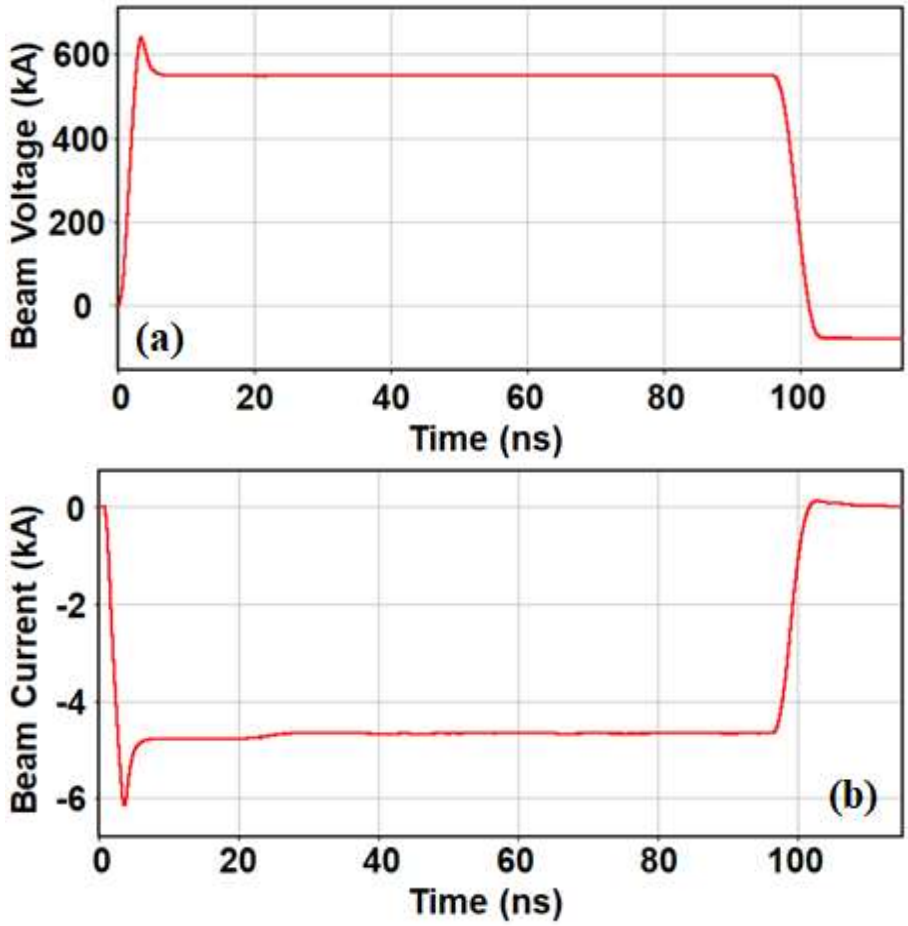

Figure 4.7: (a) DC beam voltage (550 kV) and (b) Developed electron beam current (~4.66 kA).

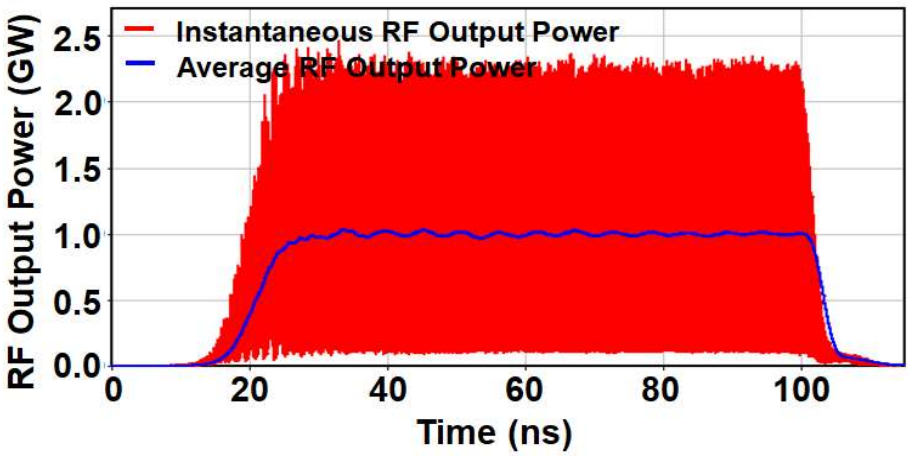

Figure 4.8: Instantaneous and average RF output power of the dual-band RBWO with sectional SWS's.

OBSERVE FFT command, which confirms one major spike in S-band at 3.6 GHz, as shown in Figure 4.9. The Frequency-Time plot confirms that the frequency generation of 3.6 GHz for the entire simulation time of 100 ns, as shown in Figure 4.10. The

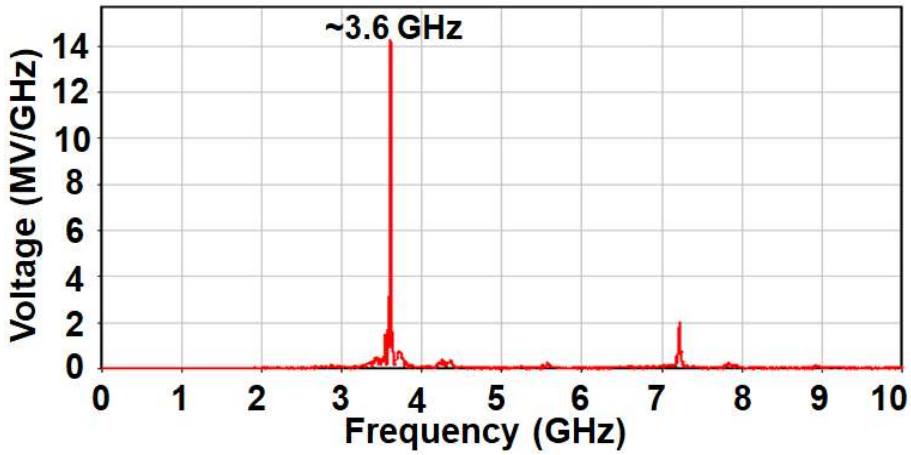

Figure 4.9: FFT of the generated HPM wave for RBWO with Sectional Bragg reflector.

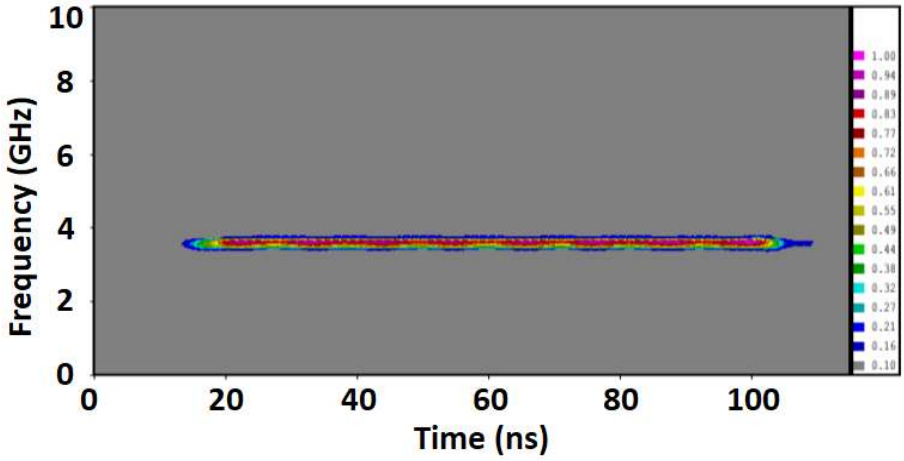

Figure 4.10: Time-Frequency plot showing generation of frequency.

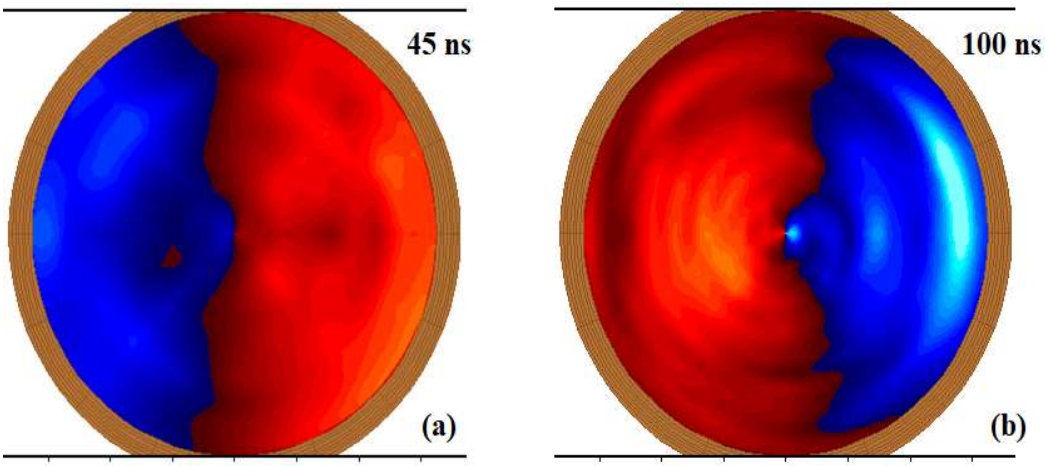

Figure 4.11: Contour plots for the generated mode for both bands at two different time instants.

snapshot of contour captured at different time instances of the simulation is shown in Figure 4.11, which shows that the two way (left and right) helically corrugated single

fold (m = 1) cylindrical waveguide outputted the linearly polarized TE_{11} mode in S-band.

4.5 Parametric Analysis

In this section, the sensitivity of the device with the magnetic field, beam voltage, and drift section length-II are studied on average RF output power, and frequency.

4.5.1 Effect on frequency and RF power with magnetic field

To investigate the generation of a maximum RF output power, the magnetic field is varied through PIC simulation, as shown in Figure 4.12. The cyclotron synchronism occurred at B_1 and B_2 that are between the cyclotron mode line and forward wave fundamental space harmonics and the cyclotron mode line and backward wave fundamental space harmonic, respectively. The cyclotron absorption of RF output power is calculated at $B_1 \approx$ 0.24 T and B_2 ranging 0.26 T - 0.6 T. The B_1 and B_2 values are well-matched with calculated values given by [125] equations (2.21) and (2.22), respectively. The two unwanted cyclotron synchronism resulted in the suppression of RF output power, as observed in Figure 4.12. The maximum and saturated RF output power is obtained at 1.3 T.

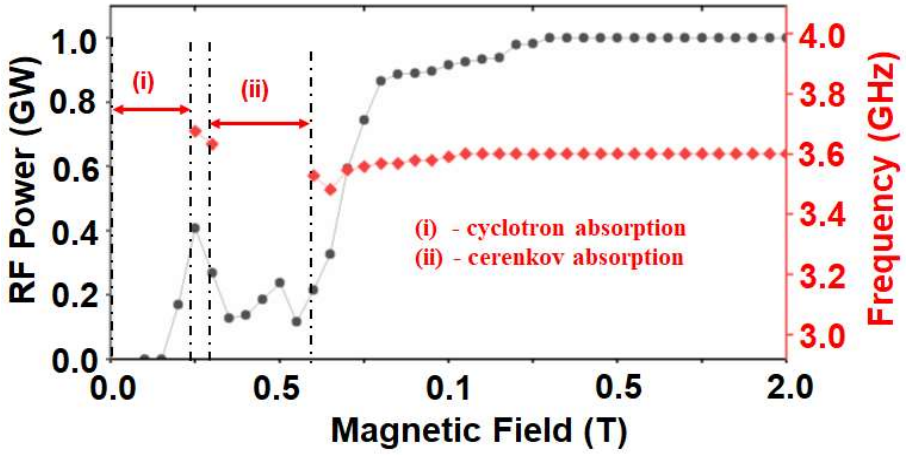

Figure 4.12: Effect of guiding magnetic field on frequency and RF power.

4.5.2 Effect on RF power with beam voltage

The RF output power pulse duration is observed over different accelerating potential. As the accelerating potential is varied from 400 kV to 900 kV, the RF output power increases up to 1.1 GW, and beyond 600 kV the RF output power pulse is become irregular and shortened, as shown in Figure 4.13. This indicates that the RF break down occurs due to high electric field inside the device, as the accelerating potential above 600 kV. Therefore, the device can be tuned smoothly from 400 to 600 kV to get a regular pulse shape.

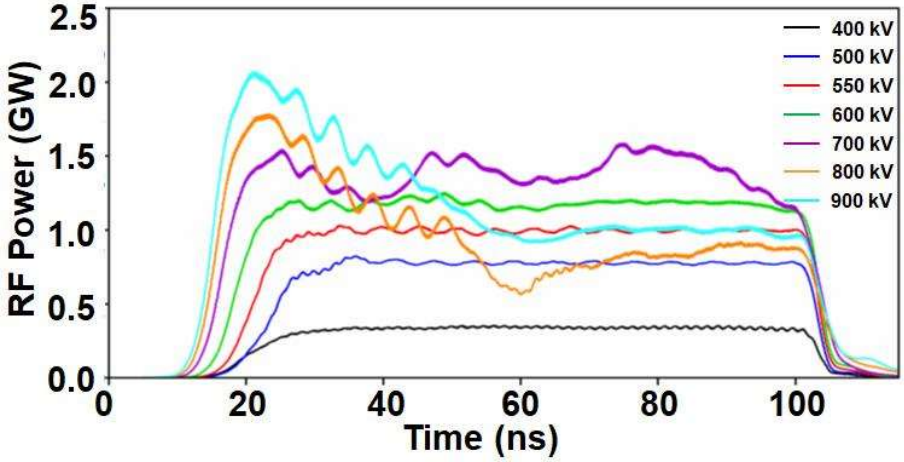

Figure 4.13: Effect of beam voltage on RF power.

4.5.3 Effect on RF output power and frequency with Drift section-II

The frequency and RF output power for different drift section-II lengths are shown in

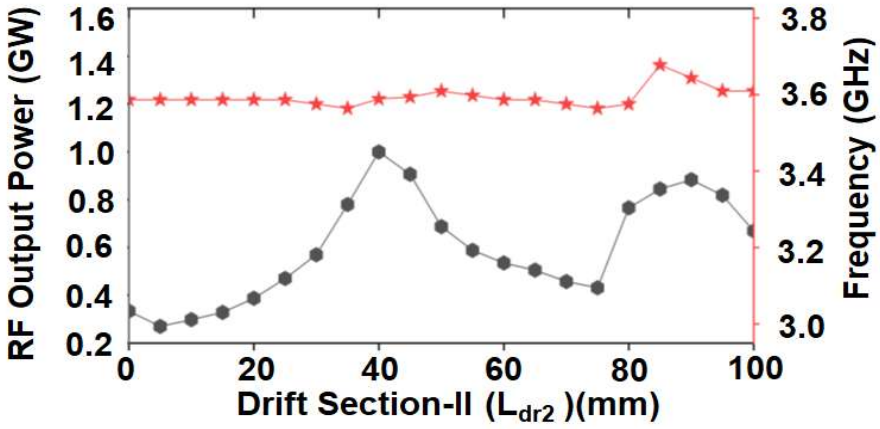

Figure 4.14: Effect of drift section length (Ldr2) on RF output power, and frequency.

Figure 4.14. Two spikes of the RF output power (blue color) were obtained due to phase synchronization of the beam and -1st space harmonic of TM_{01} mode for various optimal drift length-II (L_{dr2}) [84]. It is observed that the maximum phase synchronization is occurred for L_{dr2} = 39.00 mm. Hence a ~5 % (Figure 4.14.) tuning is achieved around the center frequency between 00.00 mm and 100 mm of the drift length.

4.6 Conclusion

The design methodology and analytical background of a sectional Bragg structure has been presented to understand its principle of operation. The sectional Bragg structure was used as an integral part of RBWO, which acted like a reflector cum mode converter. Therefore, the use of Bragg structure has eliminated the requirement of an external mode converter in a conventional RBWO. Further, the RBWO has been studied by combining the sectional Bragg structure having six periods with an S-band uniform SWS for its beam-wave interaction. The drift section between the Bragg structure has enhanced the reflection coefficient. Hence the efficiency increases up to ~39.5 %. It was observed that the RF output power depends upon the value of guiding magnetic field. Further, the frequency tuning ~5 % is observed by varying drift sections-II (L_{dr2}) length respectively.

The next Chapter is dealt with the dual-band operation of an RBWO using Sectional SWS.